Extracting a more realistic pseudopotential for aluminum, lead, niobium and tantalum from superconductor electron tunnelling spectroscopy data

Zheng, X. (2011). Extracting a more realistic pseudopotential for aluminum, lead, niobium and tantalum from superconductor electron tunnelling spectroscopy data. Journal of Physics C: Condensed Matter, submitted, 1-19.

Published in:
Journal of Physics C: Condensed Matter

Extracting a more realistic pseudopotential for aluminum, lead, niobium and tantalum from superconductor electron tunnelling spectroscopy data

X. H. Zheng and D. G. Walmsley
*Department of Pure and Applied Physics, Queen's University of Belfast, BT7 1NN, N. Ireland**
(Dated: 7 September 2011)

Electron tunnelling spectroscopy, developed to extract from superconductive metals the electron-phonon spectral density, $\alpha^2F(\nu)$, is found to be a powerful tool also for extracting a more realistic pseudopotential from such metals. The pseudopotential so extracted has a range of surprising but physically reasonable properties and regenerates $\alpha^2F(\nu)$ accurately. Free from most of its long-standing uncertainties, this pseudopotential may be useful in a number of active fields.

PACS numbers: 71.15.Dx, 74.25.Kc, 31.10.+z

I. INTRODUCTION

We identify and wish to highlight a long overlooked opportunity that allows us to extract a more realistic pseudopotential for metals. We illustrate the opportunity by examining two fcc metals (aluminum and lead) and two bcc metals (niobium and tantalum) from data already available in the superconducting state.

In simple metals the conduction electrons often appear to be affected little by the periodic potential of the atomic lattice so that their behavior is close to that of free electrons. In many applications the atomic potential can in such cases be replaced by a pseudopotential which is weak compared with the actual atomic potential particularly in the core region of the atoms [1]. Although the pseudopotential has an idealized theoretical fundation, in practice it has to be constructed as an ad-hoc model with a number of parameters adjusted until the outcome fits experimental observation. This model can be less than realistic: for example in the empty core model the potential is assumed to vanish within a certain radius from the atomic site to serve a specific purpose [2].

How can a more realistic pseudopotential be determined from experimental data? To achieve this we need to acquaint ourselves with the Eliashberg-Nambu theory of superconductivity [3], a variant of the classic superconductor theory by Bardeen, Cooper and Schrieffer (BCS) [4]. Although it allows determination of the electron-phonon spectral density, $\alpha^2F(\nu)$, from experimental electron tunnelling conductance data (electron tunnelling spectroscopy) [5], a first principles calculation of $\alpha^2F(\nu)$ is far more difficult and remains to be achieved. In such a calculation one must know the details of the atomic core potential in order to estimate the strength of the electron-phonon interaction. Common practice has been to use a model pseudopotential, developed previously to serve some other specific purpose; even in the best cases its use in Eliashberg calculations leads to $\alpha^2F(\nu)$ with unduly sharp features and high peaks [6–9] both significantly different from observation. Some authors attribute the problem to the use of single plane wave electrons [10].

However, to achieve a resolution of the issue one need not agonize over the lack of detailed knowledge of $\delta V(r)$ (pseudopotential variation across the core region of atoms) or the electron configuration that goes with it. It is more practical and useful to proceed in the opposite direction, that is to extract $\delta V(r)$ for the material by fitting trial forms of $\delta V(r)$ to the the experimental $\alpha^2F(\nu)$. Fitting is here achieved through an application previously used to fit a trial $\alpha^2F(\nu)$ with the tunnelling data [11]. With the detailed form of $\delta V(r)$ thus extracted the problem has been turned round: instead of working with an uncertain $\delta V(r)$ to determine a plausible $\alpha^2F(\nu)$, we have now used the experimentally derived $\alpha^2F(\nu)$ to calculate a more realistic $\delta V(r)$ in precise detail.

We find that the $\delta V(r)$, extracted directly from the tunnelling data, has a range of physically reasonable and somewhat surprising properties. For example in reciprocal space $\delta V(r)$ is converted into $\delta V(q)$, which is required to have the so-called long wavelength limit $-0.67\epsilon_F$ when $q \to 0$, where ϵ_F is the Fermi energy. Our $\delta V(q)$ does have this long wavelength limit but, contrary to the previous guess, is not monotonically increasing from $q = 0$ and eventually becomes positive when q is close to $2k_F$, k_F being the Fermi wavenumber. When we revert to real space, $\delta V(r)$ appears to be a sum of a number of Gaussian-like curves, which justifies the previous practice in electron energy band calculation, apparently based on experience and intuition [12, 13]. However, appearance can be deceiving, for although the Gaussian curves can be a good starting point for band calculations, it is almost impossible to recover from them the desired (more realistic) $\delta V(q)$ with the detail on which $\alpha^2F(\nu)$ sensitively depends [14].

Our article is arranged as follows. In Section II we discuss phonon dispersion curves. In Section III we discuss phonon densities of states and in Section IV the electron-phonon spectral density. In Section V we extract the more realistic pseudopotential from the tunnelling data. We use aluminum as an example in the above discussions. In Sections VI, VII and VIII we extract the more realistic

*Electronic address: xhz@qub.ac.uk

pseudopotential for lead, niobium and tantalum. A brief discussion of the results is presented in Section IX and conclusions in Section X.

II. PHONON DISPERSION

For simplicity we assume one atom per primitive cell. In the Born-von Kármán theory the equation of lattice vibration is

$$M\omega^2 u_\alpha(\mathbf{q}) = \sum_\beta C_{\alpha\beta} u_\beta(\mathbf{q}) \tag{1}$$

where $u_\alpha(\mathbf{q})$ and $u_\beta(\mathbf{q})$ are canonical displacements of atoms, $\mathbf{q}$ phonon momentum, $\alpha, \beta = 1, 2, 3$ and ω lattice vibration frequency, to be specified as $\omega_\ell(\mathbf{q})$ in accordance with the value of $\mathbf{q}$ and phonon polarization,

$$C_{\alpha\beta} = \frac{1}{2} \sum_{\mathbf{R}-\mathbf{R}'} \frac{\partial^2 V(\mathbf{R}-\mathbf{R}')}{\partial u_\alpha(\mathbf{R}) \partial u_\beta(\mathbf{R}')} \exp[-i\mathbf{q}\cdot(\mathbf{R}-\mathbf{R}')], \tag{2}$$

$u_\alpha(\mathbf{R})$ and $u_\beta(\mathbf{R}')$ (to be written as u_α and u'_β) are atomic displacements in real space, $\mathbf{R}$ and $\mathbf{R}'$ coordinates of neighboring atomic sites [15]. Letting

$$V(\mathbf{R}-\mathbf{R}') = V(r) \tag{3}$$

with $r = |\mathbf{R}-\mathbf{R}'|/a$, a being the crystal constant and $r = (x^2+y^2+z^2)^{1/2}$, we have

$$\begin{aligned}
\frac{\partial^2 V}{\partial u_1 \partial u'_1} &= \frac{1}{a^2}\left[V''(r)\frac{x^2}{r^2} - V'(r)\frac{y^2+z^2}{r^3}\right], \\
\frac{\partial^2 V}{\partial u_1 \partial u'_2} &= \frac{1}{a^2}\left[V''(r)\frac{xy}{r^2} - V'(r)\frac{xy}{r^3}\right], \\
\frac{\partial^2 V}{\partial u_1 \partial u'_3} &= \frac{1}{a^2}\left[V''(r)\frac{xz}{r^2} - V'(r)\frac{xz}{r^3}\right], \\
\frac{\partial^2 V}{\partial u_2 \partial u'_2} &= \frac{1}{a^2}\left[V''(r)\frac{y^2}{r^2} - V'(r)\frac{x^2+z^2}{r^3}\right], \\
\frac{\partial^2 V}{\partial u_2 \partial u'_3} &= \frac{1}{a^2}\left[V''(r)\frac{yz}{r^2} - V'(r)\frac{yz}{r^3}\right], \\
\frac{\partial^2 V}{\partial u_3 \partial u'_3} &= \frac{1}{a^2}\left[V''(r)\frac{z^2}{r^2} - V'(r)\frac{x^2+y^2}{r^3}\right]
\end{aligned} \tag{4}$$

which are controlled explicitly by $V'(r)$ and $V''(r)$, the first and second order derivatives of $V(r)$ with respect to its argument, respectively, that is in Eq.(4) we can at most have two independent matrix elements, which is slightly different from the previous formulation based on

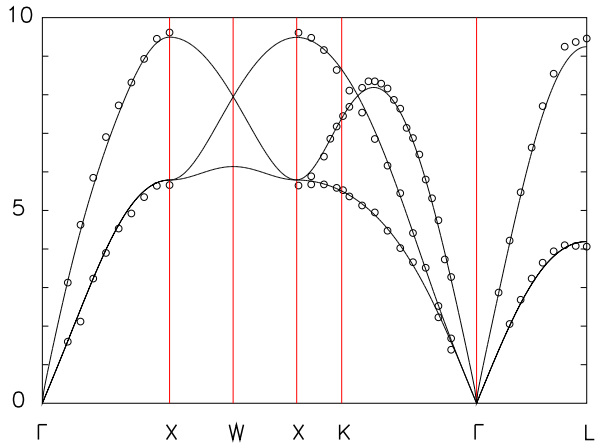

FIG. 1: Phonon dispersion curves for aluminum, open circles are experimental data by Stedman and Nilsson [18], lines from theoretical calculation, all in 10^{12} Hz ($\hbar\omega_\ell$ in 4.136 meV), equation of motion evaluated over 6 shells, crystal symmetry directions indicated with usual conventions.

symmetry of the lattice [16]. For example in the case of the bcc lattice in the direction $(a, a, 0)$ we have

$$\begin{bmatrix} \alpha_3 & \alpha_3 & \\ \alpha_3 & \alpha_3 & \\ & & \beta_3 \end{bmatrix} \quad \text{and} \quad \begin{bmatrix} \alpha_3 & \gamma_3 & \\ \gamma_3 & \alpha_3 & \\ & & \beta_3 \end{bmatrix} \tag{5}$$

from the current formulation and from [16] respectively. Woods reported that ω may become imaginary for a bcc lattice [17] which we have not encountered in our computation.

To take the effect of screening into account, we add the Thomas-Fermi potential to $V(r)$ in Eq. (3) and find that the following term

$$\frac{3}{2}\frac{N}{\Omega}\frac{Q^2}{\epsilon_0}\frac{q_\alpha q_\beta}{q^2+k_s^2} \Big/ \left[\exp\left(\frac{T_D}{T}\frac{q}{q_D}\right) - 1\right] \tag{6}$$

must be added to the matrix elements in Eq. (4), where N is the number of atoms, Ω volume of the sample, Q nuclear charge, ϵ_0 permittivity, k_s Thomas-Fermi screening wavenumber, q_D Debye wavenumber, T_D and T Debye temperature and temperature when lattice dispersion is measured.

When evaluating Eq. (1), r runs over for example 6 shells of neighboring atoms, we treat $V'(r)$ and $V''(r)$ in Eqs. (4) as parameters, which are adjusted until ω matches its measured values, shown in FIG. 1 as open circles [18]. Our adjustment of the parameters is helped by a popular method of optimization due to Hooke and Jeeves [19], which was also used extensively in order to extract $\alpha^2F(\nu)$ from the tunnelling data. This method, known as a pattern search method, includes a stage of pattern search and a stage of pattern moving. At the first stage values of $V'(r)$ and $V''(r)$ are perturbed in turn individually and, in accordance with the response

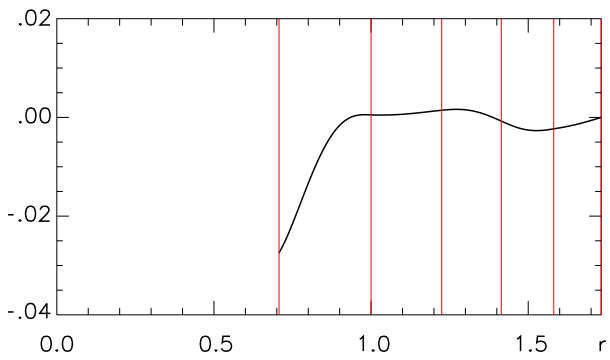

FIG. 2: Lattice potential $V(r)$ of an aluminum ion, experienced by its neighbors over a distance r, where V is in units of Fermi energy and r in units of lattice constant, vertical lines mark atomic shells of the fcc crystal.

of a penalty function, are registered as favorable perturbations or otherwise. At the second stage all the favorable perturbations are implemented simultaneously, the others are implemented in the opposite directions. This pattern motion can either be one-off or be pushed back and forth over a shortening range until the penalty function is minimized. These two steps are repeated to reach a reasonable fit between theory and experiment, as is shown in FIG. 1. Parameters in Eq. (6), including Q and k_s, are treated in a similar manner.

We construct the lattice potential, experienced by the neighbors of an atom, from $V'(r)$ and $V''(r)$ in Eqs. (4), which are evaluated only at the locations of the neighboring shells of the atom. Between these shells, we interpolate $V'(r)$ with 3-rd order polynomials, whose derivatives match the shell values of $V''(r)$. We then integrate these polynomial sections numerically and find the curve of $V(r)$ in FIG. 2, assuming $V(r) = 0$ at the outermost shell. If we substitute the expression of this curve back into Eq. (1), we can reproduce accurately the theoretical phonon dispersion curves in FIG. 1. The curve in FIG. 2 tells us nothing about the atomic potential when $r < 0.707$, where literally lies a vast playground for a theoretician to build a pseudopotential (s)he feels appropriate, if (s)he is constrained just by phonon dispersion. Indeed in [20] the empty core model is verified against phonon dispersion. Obviously we must be careful if we wish to borrow this model for the *electron*-phonon interaction in the core region of the atoms.

III. PHONON DENSITIES OF STATES

We have the following expression for the so-called frequency distribution

$$F(\nu) = \frac{\Omega}{(2\pi)^3} \sum_\ell \frac{1}{N} \int d^3\mathbf{q}\, \delta(\nu - \hbar\omega_\ell) \tag{7}$$

which is integrated over the first phonon Brillouin zone. Eq. (7) can be written as

$$F(\nu) = \left\langle \frac{1}{N\hbar} \sum_\ell \frac{\Omega}{2\pi^2} \frac{\omega^2}{v_D^3} \frac{d\omega}{d\omega_\ell} \right\rangle_{\hbar\omega_\ell = \nu} \tag{8}$$

where the angle brackets represent the average over the surface of a unit sphere. In the above expressions $\omega_\ell = \omega_\ell(\mathbf{q})$ is the phonon frequency, $\ell = 1, 2, 3$ identifies phonon polarization, v_D Debye velocity and $\omega = v_D q$ Debye frequency (this definition of ω will be used throughout from now on). We have $N\hbar F(\nu)$ as the phonon density of states which reduces to the Debye density of states when $\omega_\ell = \omega$. In this article ω is always in Hertz (or rad/s), required by Eq. (1), and ν always in eV (or meV), required by the Eliashberg-Nambu formulation, and this ensures the correct units for $F(\nu)$ in Eq. (8).

In practice we only have to perform the average in Eq. (8) over 1/48 of the surface of the unit sphere known as the irreducible section [21]. The most labor intensive part of the job is of course to find $d\omega/d\omega_\ell$, which includes generating the phonon dispersion curves, taking derivatives of the three polarization branches with respect to q and then inverting the result. An accurate numerical method of doing so was described by Gilat and Raubenheimer [21]. Here we describe our method based on physical understanding of Eq. (8), whose purpose is to find the range of $\mathbf{q}$ with $\omega_\ell(\mathbf{q})$ falling into a given range of phonon frequencies. Let δq and $\delta\omega$ be the ranges in q and ω and

$$\begin{aligned} &(0,\ \ \delta q,\ \ 2\delta q,\ \ ...,\ \ \mathcal{N}\delta q) \\ &(0,\ \ \delta\omega,\ \ 2\delta\omega,\ \ ...,\ \ \mathcal{N}\delta\omega) \end{aligned} \tag{9}$$

grids of these ranges. Here $\mathcal{N}$ represents the number of grid divisions; $\mathcal{N}\delta q$ and $\mathcal{N}\delta\omega$ must be large enough to cover all the possible values of q and ω_ℓ. Consider for example one of the dispersion curves in FIG. 1 where $\mathbf{q}$ and $\omega_\ell(\mathbf{q})$ are in fact discrete. Suppose the total number of $\mathbf{q}$ is j when the condition $n\delta\omega \le \omega_\ell(\mathbf{q}) < (n+1)\delta\omega$ is met, then we have $j\delta q$ as the number of phonon states falling into the frequency grid near $\omega = n\delta\omega$, giving $j\delta q/\delta\omega$ as the density of phonon states near $\omega_\ell = n\delta\omega$.

In FIG. 3 we show the phonon density of states of aluminum found with the above method. For comparison we also show the Debye phonon density of states, whose maximum value is $104/T_D$, T_D being the Debye temperature, giving 0.24, 0.99, 0.38 and 0.44 as maxima for aluminum, lead, niobium and tantalum, respectively, in units of 1/meV. There are small wriggles or kinks in the densities of states curves of nickel, aluminum and sodium in [21] which Gilat and Raubenheimer attributed to computer errors. It is interesting that such kinks are also evident in FIG. 3, in particular around the nearly straight top of the transverse peak; these appear to be genuine features of the phonons. Indeed we find similar features when we calculate phonon densities of states for

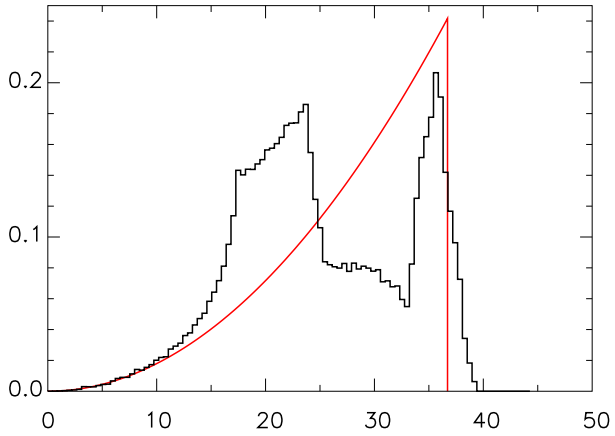

FIG. 3: Frequency distribution $F(\nu)$ for aluminum (histogram, in 1/meV) against ν (in meV), Debye distribution shown as a smooth curve (color online).

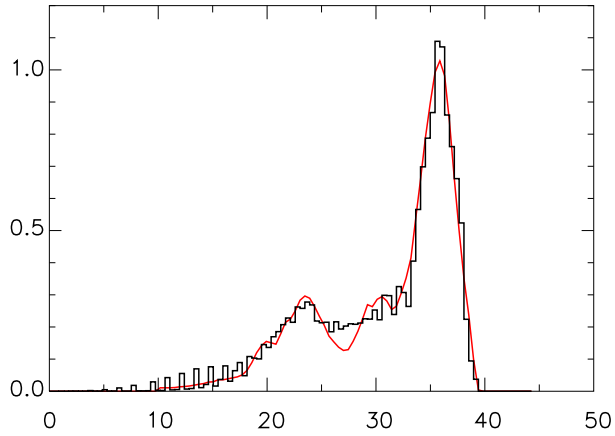

FIG. 4: Electron-phonon spectral density $\alpha^2F(\nu)$ of aluminum (histogram, dimensionless, $\lambda = 0.52$) against ν (in meV), experimental $\alpha^2F(\nu)$ shown as a smooth curve (color online, $\lambda = 0.50$).

nickel and sodium. It is also interesting that in our calculations aluminum and nickel (both fcc crystals) resemble each other closely in their density of states distributions, whereas the resemblance is not so obvious in [21]. The longitudinal peak in FIG. 3 is not as prominent as that in [21] but comparable with the experimental peaks in [18] and [22]. There is just 0.7% difference when we compare the value of specific heat from the phonon state distribution in FIG. 3 with the Debye value. The volume of our calculations is rather modest (29,900 values of $\mathbf{q}$).

IV. ELECTRON-PHONON SPECTRAL DENSITY

The familiar formula for the electron-phonon spectral density (sometimes known as the Eliashberg or Eliashberg-Nambu function) is of the following form:

$$\alpha^2F(\nu) = \left\langle \frac{\Omega}{(2\pi)^3} \sum_\ell \int d^2\mathbf{k}' \frac{|g_\ell(\mathbf{q})|^2}{\hbar v_F} \delta(\nu - \hbar\omega_\ell) \right\rangle \quad (10)$$

where the two dimensional integration with respect to $\mathbf{k}'$ is over the Fermi surface, $\mathbf{q} = \mathbf{k}' - \mathbf{k}$ and the angle brackets represent the average with respect to $\mathbf{k}$, also over the Fermi surface. In Eq. (10) v_F is the Fermi velocity, $g_\ell(\mathbf{q})$ matrix element of electron-phonon scattering which, in the case of a spherical Fermi surface, leads to

$$\alpha^2F(\nu) = \frac{3}{4}\left(\frac{2}{Z}\right)^{1/3} \frac{m}{M} \left(\frac{T_F}{T_D}\right)^2 \times \frac{1}{2\pi} \int_0^{2\pi} d\phi \sum_\ell e_\ell^2 \frac{\omega}{\omega_\ell} \frac{d\omega}{d\omega_\ell} \left[\frac{q}{q_D} \frac{\delta V(q)}{\epsilon_F}\right]^2_{\hbar\omega_\ell = \nu} \quad (11)$$

where for simplicity we have dropped the angle brackets in Eq. (10), that is we assume the initial state $\mathbf{k}$ has no effect on $\alpha^2F(\nu)$ in the above expression. In Eq. (11) $\mathbf{k}$ is placed in the center of the (q, θ, ϕ) coordinates so that $q = 2k_F \sin(\theta/2)$ [23], Z is the valency, m and M electronic and atomic mass, respectively, and T_F and ϵ_F Fermi temperature and energy.

The similarities between Eq. (8) and Eq. (11) are apparent, but now we have to weight $d\omega/d\omega_\ell$ with e_ℓ^2 and $\delta V(q)$, which means that the histogram in FIG. 3 will have to be distorted. The force constant matrix in Eq. (1) can be written as:

$$U^T \begin{bmatrix} M\omega_1^2 & & \\ & M\omega_2^2 & \\ & & M\omega_3^2 \end{bmatrix} U \quad (12)$$

where U is an orthogonal unitary matrix and

$$\begin{bmatrix} e_1 \\ e_2 \\ e_3 \end{bmatrix} = q^{-1} U \begin{bmatrix} q_1 \\ q_2 \\ q_3 \end{bmatrix} \quad (13)$$

defines e_ℓ in Eq. (11), $q_1^2 + q_2^2 + q_3^2 = q^2$. Apparently we have $e_1^2 + e_2^2 + e_3^2 = 1$, that is (e_1, e_2, e_3) is a unit vector marking phonon polarization, which makes major differences between the outcomes of Eqs. (8) and (11). It is well known that transverse phonons do not interact with electrons [23]. If we restrict the phonon momentum $\mathbf{q}$ in Eq. (10) to the first Brillouin zone, then the transverse peaks in FIG. 3 will all but disappear, resulting in theoretical values of $\alpha^2F(\nu)$ comparing poorly with experimental data. The practice of extending the upper value of q in Eq. (11) to $2k_F$ [14] brings the transverse peaks back and makes the longitudinal peak higher relative to the transverse peaks but the resulting $\alpha^2F(\nu)$ still compares poorly with experimental data.

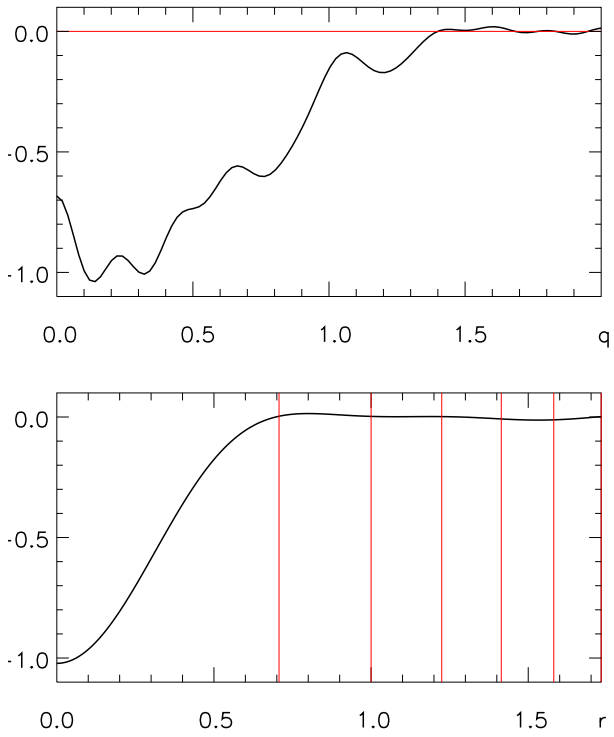

FIG. 5: More realistic pseudopotential for aluminum, in units of Fermi energy, in reciprocal space (upper, q in units of k_F and the horizontal line marks $\delta V = 0$) and real space (lower, r in units of lattice constant, vertical lines mark atomic shells).

V. MORE REALISTIC PSEUDOPOTENTIAL

In our derivation we let

$$\sum_{\mathbf{R}} V(\mathbf{r}-\mathbf{R}) \tag{14}$$

be the crystal potential, $\mathbf{r}$ being the electronic coordinates and $\mathbf{R}$ coordinates of atomic sites. We have $\delta V(r) = V(r) - V(r_1)$, $r = |\mathbf{r}-\mathbf{R}|$, r_1 being the value of r when $V(r)$ can be assumed to have reduced to its asymptotic value away from the atomic site. For simplicity we assume $V(\mathbf{r}-\mathbf{R})$ is symmetric with respect to $\mathbf{R}$ so that r_1 becomes a constant. In our formulation r_1 may become larger than r_0, the radius of the Wigner-Seitz cell. We are reminded that here the atomic potential is experienced by electrons rather than neighboring atoms so that $V(r)$ in Eq. (14) is different from $V(r)$ in Eq. (3). We will remind the reader about the nature of $V(r)$ in cases where confusion may arise. We have

$$\delta V(q) = \frac{3}{r_0^3}\int_0^{r_1} \delta V(r) j_0(qr) r^2 dr \tag{15}$$

which is the Fourier transform of $V(r)$, j_0 being a spherical Bessel function. Conversely we have

$$\delta V(r) = \frac{3}{q_D^3}\int_0^{2k_F} \delta V(q) j_0(qr) q^2 dq \tag{16}$$

which converts $V(q)$ back into real space. Here we assume $\delta V(q)$ vanishes when $q > 2k_F$ which will be justified by our numerical results in the following discussions.

We see from Eq. (11) that $\alpha^2 F(\nu)$ is proportional to the square of $\delta V(q)$. This suggests that, with a technique similar to inverse Fourier transform, we may find a more realistic atomic potential that leads accurately through Eq. (11) to the experimentally observed values of $\alpha^2 F(\nu)$. However in Eq. (11) the relation between ν and q is complicated, so that our technique to extract $\delta V(q)$ will not be a straightforward application of inverse Fourier transformation. Instead we use the method of pattern search described in Section II, modified to suit the nature of the problem.

Our penalty function for optimization measures the difference between theoretical and experimental $\alpha^2 F(\nu)$, shown in FIG. 4 as the histogram and smooth curve respectively. We resolve the atomic potential difference in reciprocal space into the following Fourier series

$$\delta V(q) = \frac{A_0}{2} + \sum_{n=1}^{20} A_n \cos\left(\frac{n\pi q}{2k_F}\right) \tag{17}$$

considering that in Eq. (11) the value of q never exceeds $2k_F$. Initially $\delta V(q)$ and hence $A_0, A_1, ..., A_{20}$ are found from a square atomic potential well (radius $= r_0$) that leads through the Mott-Jones formula (Einstein phonons) to the known value of resistivity of the metal [23]. In about 100 rounds of pattern search and moving the value of the penalty function continues to drop and the theoretical and experimental $\alpha^2 F(\nu)$ become close to each other, as can be seen from FIG. 4. From the following formula [10]

$$\lambda = 2\int_0^{\infty} \alpha^2 F(\nu)\frac{d\nu}{\nu} \tag{18}$$

we find $\lambda = 0.52$ and 0.50 for the theoretical and experimental $\alpha^2 F(\nu)$ respectively. It is not difficult to work out from FIGs. 3 and 4 the shape of the function $\alpha^2(\nu)$ which evidently will not be even close to a constant or a straight line.

In order to accelerate the above time-consuming process of optimization, we notice that, apart from $\delta V(q)$, we do not have to change any quantity in Eq. (11) when we evaluate $\alpha^2 F(\nu)$ again and again in the process of optimization. We calculate all the phonon frequencies just once and store the results for later use, saving a significant amount of computation time.

In the upper part of FIG. 5 we show the more realistic pseudopotential in reciprocal space, $\delta V(q)$, reached after the above process of optimization. In the range $1.5k_F < q < 2k_F$ values of $\delta V(q)$ become vanishingly small, as a natural outcome of optimization. We have $\delta V(q) \to -0.69\epsilon_F$ when $q \to 0$ which also is a natural outcome, close to the theoretical value $-0.67\epsilon_F$ for the long wavelength limit of the pseudopotential.

In the lower part of FIG. 5 we show the more realistic pseudopotential in real space, $\delta V(r)$, which is found

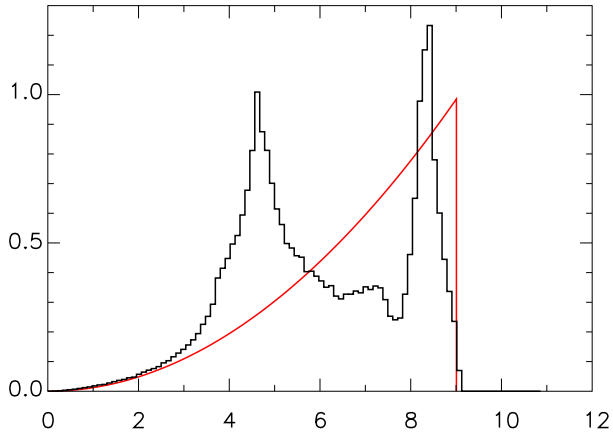

FIG. 6: Frequency distribution $F(\nu)$ for lead (histogram, in 1/meV) against ν (in meV), Debye distribution shown as a smooth curve (color online).

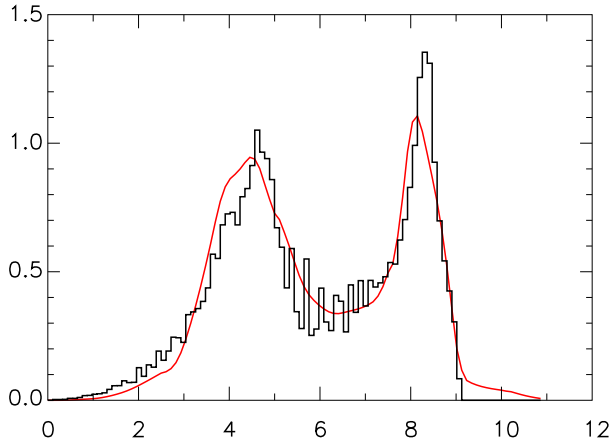

FIG. 7: Electron-phonon spectral density $\alpha^2F(\nu)$ of lead (histogram, dimensionless, $\lambda = 1.58$) against ν (in meV), experimental $\alpha^2F(\nu)$ shown as a smooth curve (color online, $\lambda = 1.48$).

through Eq. (16). This real space potential looks very much like a Gaussian curve within the first atomic shell. However, it is very difficult, if not impossible, for us to construct from intuition a Gaussian curve that would lead through Eq. (15) to $\delta V(q)$ in the upper part of FIG. 5 with so much detail. It is worth noting that, beyond the first atomic shell, the atomic potentials in FIGs. 2 and 5 for ions and electrons respectively might be consistent, knowing that ions can see a stronger potential on account of their greater nuclear charges.

VI. LEAD

Theoretical calculation of phonon dispersion with the Born-von Kármán model for lead has always been a challenge. The phonon state distribution found by Gilat in

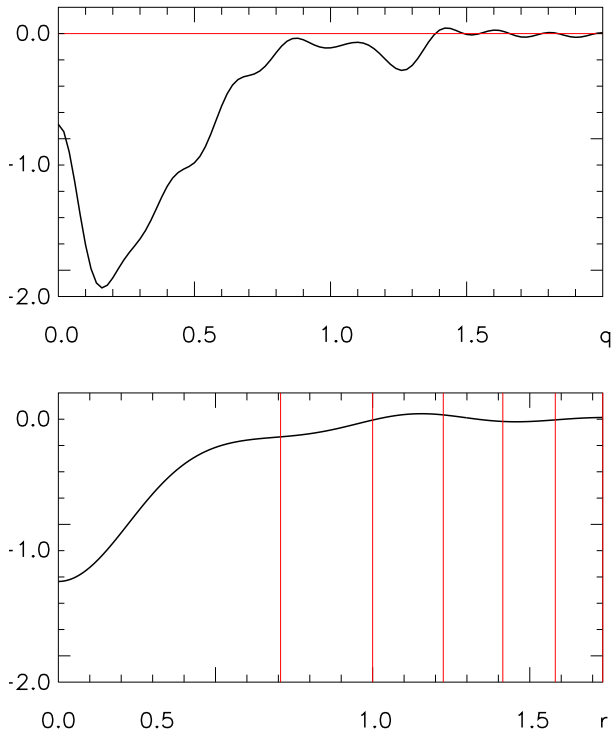

FIG. 8: More realistic pseudopotential for lead, in units of Fermi energy, in reciprocal space (upper, q in units of k_F and the horizontal line marks $\delta V = 0$) and real space (lower, r in units of crystal constant, vertical lines mark atomic shells).

1965 has a rather unusual feature of a lower longitudinal peak compared with the first transverse peak [24]. In 1967 Stedman, Almqvist and Nilsson measured neutron scattering from lead with exceptionally numerous **q** vectors, in order to skip the Born-von Kármán model and extract the phonon density of states directly from the scattering data [25]. The longitudinal peak turned out to be modestly higher than the first transverse peak. In 1973 Cowley used the Born-von Kármán model and data in [25] to calculate lead phonon dispersion, with 2,030,100 phonon frequencies within the irreducible section, and found again the lead phonon density of states distribution [26]. The longitudinal peak turned out to be almost twice as high as the first transverse peak. His result was used by Tomlinson and Carbotte to calculate $\alpha^2F(\nu)$ for lead [6].

We too sample the neutron scattering data from [25] along the symmetric directions of the lead crystal, more or less in the places of the open circles in FIG. 1. We follow the procedure described in Section II to find the force constant matrix, which enables us to calculate phonon frequencies in all directions in the irreducible section, which in turn enables us to evaluate the phonon density of states for lead. We show our result in FIG. 6 which can be compared with the experimental density of states distribution in [25]. We have a discrepancy of 2.4%, compared with the Debye value, when we evaluate specific

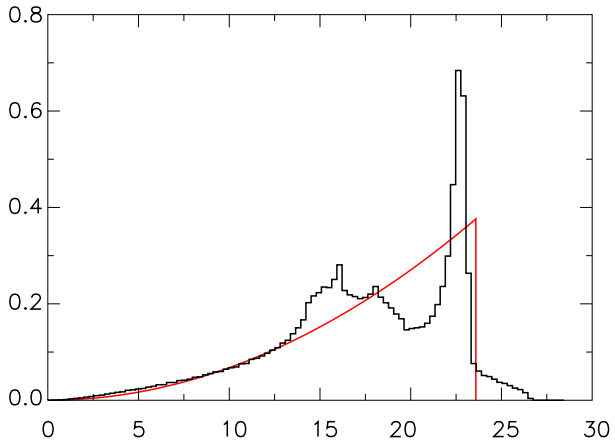

FIG. 9: Frequency distribution $F(\nu)$ for niobium (histogram, in 1/meV) against ν (in meV), Debye distribution shown as a smooth curve (color online).

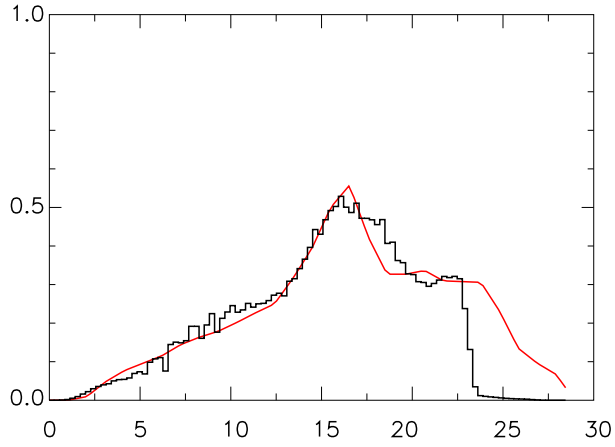

FIG. 10: Electron-phonon spectral density $\alpha^2F(\nu)$ of niobium (histogram, dimensionless, $\lambda = 0.89$) against ν (in meV), experimental $\alpha^2F(\nu)$ shown as a smooth curve (color online, $\lambda = 0.93$).

heat for lead with the curve in FIG. 6, which again arises from just 29,900 values of phonon momentum.

We follow the procedure in Section V to search for the more realistic pseudopotential for lead. The initial $\delta V(q)$ is from a square potential well (radius = r_0) that leads through the Mott-Jones formula (Einstein phonons) [23] to the known value of resistivity of lead [23]. It took about 100 rounds of pattern search and moving for us to reach the more realistic potential, which leads through Eq. (11) to $\alpha^2F(\nu)$ (histogram) in FIG. 7. It is interesting but mostly coincidental that in FIGs. 6 and 7 the histograms of $F(\nu)$ and $\alpha^2F(\nu)$ appear to be in proportion, giving the impression that $\alpha^2(\nu)$ could be a constant. Indeed in an early work by Scalapino, Schrieffer and Wilkins [27] the two peaks in FIG. 7 are approximated with two Lorentzians, weighted by $\alpha^2(\nu_1)$ and $\alpha^2(\nu_2)$, respectively, ν_1 and ν_2 being center frequencies of the first transverse peak and longitudinal peak in FIG. 6. Trial ratios of $\alpha^2(\nu_1)/\alpha^2(\nu_2) = 1$ and 0.5 were tested. We see from FIGs. 6 and 7 good reasons for these ratios to be tested. But we also see from FIGs. 3 and 4 little reason to use these ratios in general.

We show the more realistic pseudopotential for lead in reciprocal space, $\delta V(q)$, in the upper part of FIG. 8. We have $\delta V(q) \to 0.67\epsilon_F$ when $q \to 0$, which is imposed in this case only as a required physical condition for optimization. Without this condition $\delta V(0)$ will grow to become positive and large, if the calculation is left to run for a very long time, probably because of attempts to suppress the remaining difference between theoretical and experimental $\alpha^2F(\nu)$ in FIG. 7. In FIG. 8 $\delta V(q)$ becomes vanishingly small when $q > 1.5k_F$. We see from the lower part of that figure that $\delta V(r)$, found from $\delta V(q)$ through Eq. (16), appears to be a sum of a number of Gaussian curves.

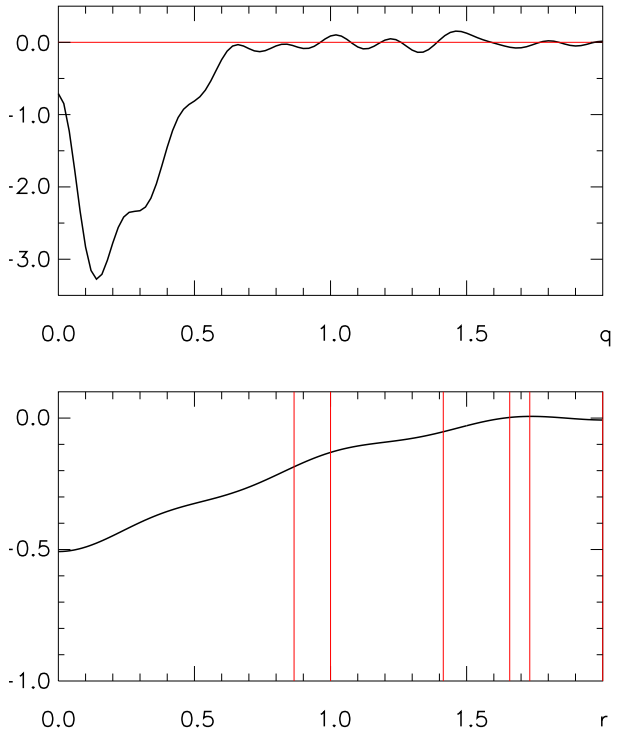

FIG. 11: More realistic atomic pseudopotential for niobium, in units of Fermi energy, in reciprocal space (upper, q in units of k_F and the horizontal line marks $\delta V = 0$) and real space (lower, r in units of lattice constant, vertical lines mark atomic shells). The scale of the upper part has been extended to accommodate the deeper potential well of niobium in reciprocal space.

VII. NIOBIUM

For niobium, the first of two bcc metals, we sample the data of neutron scattering from [28] by Nakagawa and Woods. We construct the force constant matrices in Eqs. (2) and (4) through the procedure of optimization in Section II. We evaluate Eq. (1) with 29,900 phonon momenta in the irreducible section which enables us to evaluate the frequency distribution, $F(\nu)$, in Eqs. (7) and (8). We show the result in FIG. 9, which can be compared with $F(\nu)$ in [28]. The first transverse peak and longitudinal peak are less prominent, compared with the peaks in [28], and $F(\nu)$ leads to a value of specific heat differing from the Debye value by just 0.5%.

On account of the importance of niobium in superconductivity, there have been a number of attempts to measure $\alpha^2F(\nu)$ for this metal experimentally. The measurement by Rowell and Robinson can be found from a number of references for example in [7]. The independent measurement by Bostock et al. [29] leads to negative λ and attracted some discussion in the literature [30]. Kihlstrom, Collins and Park measured $\alpha^2F(\nu)$ for thin film niobium as a function of film thickness with results generally in accord with the Rowell and Robinson measurement [31]. We therefore sample the experimental $\alpha^2F(\nu)$ by Rowell and Robinson in [7] in order to find the more realistic pseudopotential.

We follow the procedure in Section V to optimize $\delta V(q)$. We start with a square potential well (radius $= r_0$), leading through the Mott-Jones formula (Einstein phonons) to the known resistivity of niobium [23], and find the initial $\delta V(q)$ through Eq. (15). Again it takes about 100 rounds of pattern search and moving for us to reach the more realistic potential, which is shown in FIG. 10, where for clarity any numerical value of $\alpha^2F(\nu)$ has been averaged with its two immediate neighbors, in order to smooth out the spike-like features seen in the middle of the curve in FIG. 7.

In general in FIG. 10 the theoretical $\alpha^2F(\nu)$ (histogram) matches its measured values (smooth curve) reasonably well towards the long wavelength end. Towards the short wavelength end the prominent longitudinal phonon peak in FIG.9, characteristic of calculated values for a bcc metal, has been attenuated successfully. The difference between the histogram and the smooth curve beyond $\nu \simeq 23$ meV, however, appears to be from the phonon model. In FIG. 10 the experimental $\alpha^2F(\nu)$ cuts off at about 30 meV, but in FIG. 9 the phonon distribution cuts off at about 27 meV. The phonon distribution of Nakagawa and Woods in [28] also cuts off at about 27 meV. The theoretical $\alpha^2F(\nu)$ in [7] and [32], also featuring unrealistically significant peaks in both cases, cuts off earlier compared with the experimental $\alpha^2F(\nu)$, although this difference appears to be insignificant in the presence of the significant peaks. Perhaps the real phonon distribution in niobium is somewhat different from the current theoretical values.

In the upper part of FIG. 11 we show the more realistic pseudopotential in reciprocal space, $\delta V(q)$, which drops deeper compared with the corresponding pseudopotentials of aluminum and lead in FIGs. 5 and 8. The long wavelength limit of the potential in FIG. 11 is $-0.7\epsilon_F$ which emerges naturally from numerical calculation and is not far away from the theoretical limit $-0.67\epsilon_F$. In the lower part of FIG. 11 we show the more realistic atomic potential in real space, $\delta V(r)$, found from the reciprocal potential through Eq. (16). This potential again appears to be a superposition of a number of Gaussian curves. Note that the differences in the locations of the atomic shells between FIG. 11 and FIGs. 5 or 8, are due to the difference between bcc and fcc crystals.

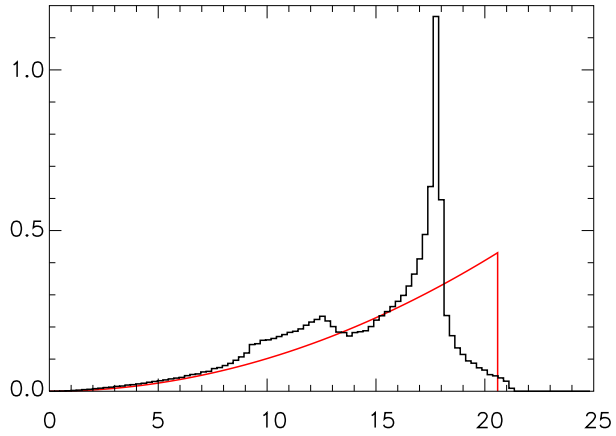

FIG. 12: Frequency distribution $F(\nu)$ for tantalum (histogram, in 1/meV) against ν (in meV), Debye distribution shown as a smooth curve (color online).

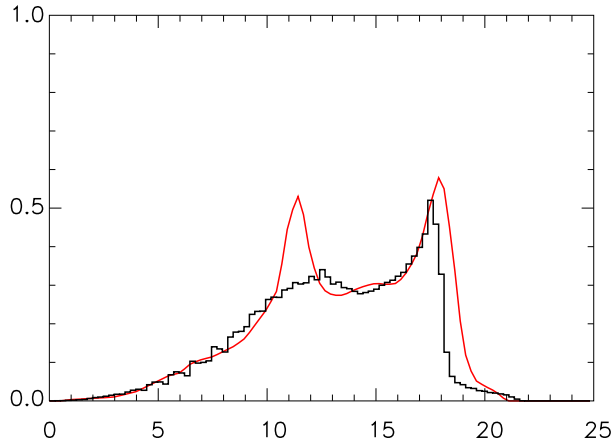

FIG. 13: Electron-phonon spectral density $\alpha^2F(\nu)$ of tantalum (histogram, dimensionless, $\lambda = 0.61$) against ν (in meV), experimental $\alpha^2F(\nu)$ shown as a smooth curve (color online, $\lambda = 0.67$).

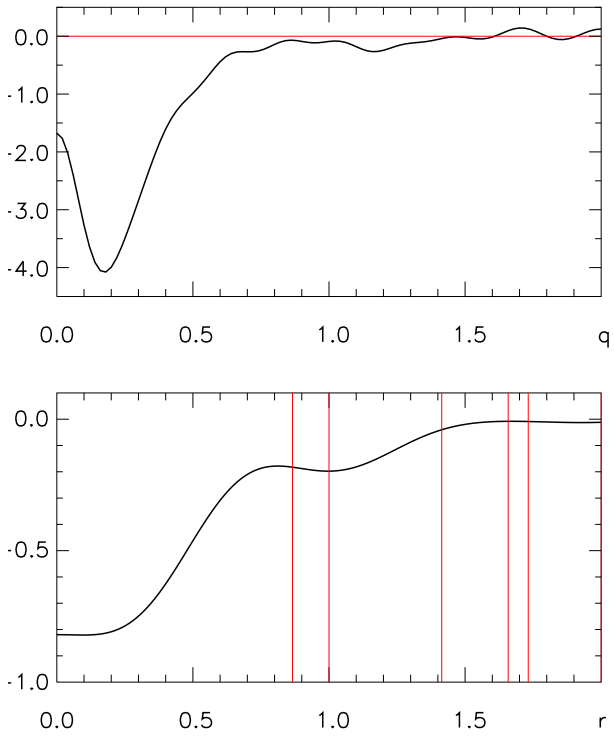

FIG. 14: More realistic atomic pseudopotential for tantalum, in units of Fermi energy, in reciprocal space (upper, q in the unit of k_F and the horizontal line marks $\delta V = 0$) and real space (lower, r in units of lattice constant, vertical lines mark atomic shells). The scale of the upper part has been extended to accommodate the deeper potential well of niobium in reciprocal space.

VIII. TANTALUM

In 1964 Woods measured inelastic neutron scattering from tantalum in the $(0, 0, a)$, $(a, a, 0)$ and (a, a, a) directions and commented that some peculiarities emerged when the Born-von Kármán model was applied to fit the neutron data [17]. In 1970 Shen [33] measured the tunnelling current from tantalum and inverted the data to find the experimental $\alpha^2F(\nu)$. In 1981 Wolf et al. [34] performed proximity electron tunnelling measurement on tantalum, yielding experimental $\alpha^2F(\nu)$ consistent with that in [33]. In 1987 Al-Lehaibi, Swihart, Butler and Pinski [8] calculated theoretical $\alpha^2F(\nu)$ for tantalum, based on Korringa-Kohn-Rostoker energy bands, Born-von Kármán phonons and the rigid muffin tin model for the electron-phonon matrix element. The result features with significant high peaks not seen from the experimental $\alpha^2F(\nu)$.

Here we use the neutron scattering data in [17] to generate the force constant matrices in Section II via the optimization procedure described in that section. The matrices are evaluated over 6 atomic shells. The optimization procedure allows us to include more shells, but the benefit was not apparent. We then proceed to search for the more realistic pseudopotential, through the procedure described in Section V. We use the experimental $\alpha^2F(\nu)$ in [33] to generate the penalty function. Initially $\delta V(r)$ is a square potential (radius $= r_0$) that leads through the Mott-Jones formula (Einstein phonons) to the known value of resistivity of tantalum [23]. We reached the more realistic potential after about 100 rounds of pattern search and moving.

We see from FIG. 12 that in general our calculated phonon density of states distribution is consistent with the distribution determined directly from experiment in [17], in particular with respect to the sharp and high longitudinal peak, although the use of arbitrary units in [17] makes quantitative comparison difficult. The transverse phonon peaks, however, are less strong in our distribution. Our distribution leads to just a 0.9% difference in specific heat compared with the Debye value.

We see from FIG. 13 a fair comparison between the calculated (histogram) and experimental values of $\alpha^2F(\nu)$ (smooth curve). In particular the significant $\alpha^2F(\nu)$ peaks in [8] have been attenuated. The remaining difference between the two curves in FIG. 13 appears to be from our phonon model in Section II, which is based on a simple idea of the central force and Thomas-Fermi screening. Perhaps a more sophisticated treatment of the atomic force is needed, in order to reproduce the experimental $\alpha^2F(\nu)$ more accurately. For clarity any numerical value of $\alpha^2F(\nu)$ in FIG.13 has been averaged with its two immediate neighbors.

We see from the upper part of FIG. 14 that the more realistic pseudopotential in reciprocal space, $\delta V(q)$, has a long wavelength limit $-1.6\epsilon_F$, which is a natural outcome of optimization, reflecting perhaps the noticeable difference between the histogram and smooth curve towards the short wavelength end in FIG. 13. We can redesign the penalty function to impose the theoretical long wavelength limit, $-0.67\epsilon_F$, on $\delta V(q)$, with other values of $\delta V(q)$ being changed slightly as a consequence. Fitting in FIG. 13 might become slightly worse. However at our current stage of discussion there is no urgent need for us to do so. We see from the lower part of FIG.14 that the more realistic pseudopotential in real space, $\delta V(r)$, is apparently close to a sum of a number of Gaussian curves.

IX. DISCUSSION

Like many noticeable or significant advances in physics, the pseudopotential started as a theoretical convenience with an element of arbitrariness, demonstrated by for example the apparently less than realistic empty core model. In 1952 Parmenter studied electron energy bands in lithium, atomic potential modelled by a sum of four Gaussian curves [12]. It has become a routine exercise in band calculation to employ the so-called Gaussian orbital in a variational formulation [13], which too is a sum of Gaussian curves (can be seen as the product of a Gaus-

sian potential and the usual electron orbital). Now we see from the lower part of FIGs. 5, 8, 11 and 14 that the pseudopotential in real space revealed by electron tunnelling spectroscopy are indeed close to a sum of Gaussian curves, which is a good indication that the pseudo potential is not just a theoretical convenience but physical reality backed by direct experimental detection and scrutiny.

Further scrutiny may help us to understand superconductivity. For example in 1989 Kihlstrom, Collins and Park measured $\alpha^2F(\nu)$ for niobium films with 30, 45, 80 and 900Å thicknesses [31]. These allow us to reveal formal changes in the core potential as a function of film thickness. More realistic potential changes may be revealed in association with changes in phonons in thin films. Another example is lithium, whose transition temperature is less than 0.4mK at ambient pressure [35] and as high as 20K under pressure [36]. Phonon properties of lithium under pressure were studied by Kasinathan, Koepernik, Kuneš, Rosner and Pickett in 2007 [37]. We may gain very interesting insight into lithium as a superconductor once $\alpha^2F(\nu)$ of the metal is measured. Iron becomes a superconductor below 2K at pressures between 15 and 30GPa [38]. Phonon dispersion of bcc iron up to 10GPa has been studied by Klotz and Braden in 2000 [39]. This may also help us to understand iron once we know the experimental $\alpha^2F(\nu)$ of the metal.

An accurate pseudopotential may further our understanding about matters beyond superconductivity, by serving as a window which allows us to reveal the electronic structure of metals in a number of fortunate cases. In 1976 Tomlinson and Carbotte calculated electric resistivity for lead and dilute lead alloys [40]. The formula employed involves $\alpha^2F(\nu)$ and the pseudopotential arises from the empty core model in [41]. In 1981 Pinski, Allen and Butler calculated electrical and thermal resistivity of niobium and palladium [42]. The formulae employed also involve $\alpha^2F(\nu)$ and the atomic potential arises from the rigid muffin tin approximation for electron energy band calculation, which was described by the authors as somewhat uncontrolled, apparently because in band calculation the electrons must be Bloch waves with many high harmonic components, compared with the single plane wave electron in the Eliashberg-Nambu formalism [32]. Now we have the pseudopotential from this very formalism and may expect a more accurate and very interesting result for electric resistivity.

In this article we have used the single plane wave electron formulation throughout consistently. We might expect a consolidation of the pseudopotential with electron energy band calculations if we switched to Bloch electrons (Leung, Carbotte, Taylor and Leavens made an attempt in this direction in 1976 in [43]).

X. CONCLUSION

We have shown that in the case of superconducting metals, for which the experimental electron-phonon spectral density $\alpha^2F(\nu)$ is available, it is possible to extract the pseudopotential $\delta V(r)$, sensed directly by the conduction electrons. It is more realistic than previous ad-hoc models and has a range of surprising but physically reasonable properties. In particular $\delta V(r)$ is exposed as having a form very much like a sum of Gaussian-like contributions at spatial intervals comparable with the lattice shell spacings. Its Fourier transform, $\delta V(q)$, though more structured than expected, shares remarkably consistent common features among the four sample metals. In general $\delta V(q)$ tends to the theoretical prediction, $-0.67\epsilon_F$, when $q \to 0$. When q increases it always evolves non-monotonically via a deep valley (often lower than $-3\epsilon_F$) before ultimately vanishing at and beyond $q = 2k_F$. Can we expect a similar behavior of $\delta V(q)$ from other metals or alloys, such as the exemplary yet exotic metal lithium? Can we extract a more realistic $\delta V(r)$ from non-superconducting materials? To what extent can we use it to probe matter? These and other questions invite further study.

[1] J. C. Phillips and L. Kleinman, Phys. Rev. **116**, 287 (1959).

[2] E. Fermi, Nuovo Cimento **2**, 157 (1934). H. Hellmann, Acta Physichemica URSS **1**, 913 (1935). W. Kassatptschkin, J. Chem. Phys. **4**, 324 (1936).

[3] L. P. Gokov, Sov. Phys. JETP **7**, 505 (1958). A. B. Migdal, Sov. Phys. JETP **7**, 996 (1958). G. M. Eliashberg, Sov. Phys. JETP **11**, 696 (1960). Y. Nambu, Phys. Rev. **117**, 648 (1960). J. R. Schrieffer, D. J. Scalapino and J. W. Wilkins, Phys. Rev. Lett. **10**, 336 (1963). D. J. Scalapino, J. R. Schrieffer and J. W. Wilkins, Phys. Rev. **148**, 263 (1966). Y. Wada, Phys. Rev. **135**, A1481 (1964). V. Ambegaokar and L. Tewordt. Phys. Rev. **134**, A805 (1964).

[4] J. Bardeen, L. N. Cooper and J. R. Schrieffer, Phys. Rev. **108**, 1175 (1957).

[5] E. L. Wolf (ed), Principles of electron tunnelling spectroscopy (Oxford Univ. Press, Oxford, 1985).

[6] P. G. Tomlinson and J. P. Carbotte, Phys. Rev. B **13**, 4738 (1976).

[7] W. H. Butler, H. G. Smith and N. Wakabayashi, Phys. Rev. Lett. **39**, 1004 (1977).

[8] A. Al-Lehaibi, J. C. Swihart, H. Butler and F. J. Pinski Phys. Rev. B **36**, 4103 (1987).

[9] S. Y. Savrasov and D. Y. Savrasov, Phys. Rev. B **54**, 16487 (1996).

[10] J. P. Carbotte, Rev. Mod. Phys. **62**, 1027 (1990).

[11] X. H. Zheng and D. G. Walmsley, Phys. Rev. B **76**, 224520 (2007).

[12] R. H. Parmenter, Phys. Rev. **86**, 552 (1952).

[13] S. P. Singhal and J. Callaway, Phys. Rev. B **16**, 1744 (1977).

[14] J. P. Carbotte and R. C. Dynes, Phys. Rev. **172**, 476 (1968).

[15] M. Born and K. Huang, Dynamical theory of crystal lattices (Clarendon, Oxford, 1954).

[16] A. D. B. Woods, Inelastic scattering of neutrons in solids and liquids (International Atomic Energy Agency, Vienna, 1963), vol. II, p. 1.

[17] A. D. B. Woods, Phys. Rev. **136**, A782 (1964).

[18] R. Stedman and G. Nilsson, Phys. Rev. **145**, 492 (1966).

[19] R. Hooke and T. A. Jeeves, J. Assn. Computing Machinery **8**, 212 (1961).

[20] W. A. Harrison, Pseudopotentials in the theory of metals (W. A. Benjamin, New York 1966).

[21] G. Gilat and L. J. Raubenheimer, Phys. Rev. **144**, 390 (1966).

[22] M. Kresch, M. Lucas, O. Delaire, J. Y. Y. Lin and B. Fultz, Phys. Rev. B **77**, 024301 (2008).

[23] N. F. Mott and H. Jones, The theory of the properties of metals and alloys (Dover, New YOrk, 1958), p254, 257, 264.

[24] G. Gilat, Solid Stat. Commu. **3**, 101 (1965).

[25] R. Stedman, L. Almqvist and G. Nilsson, Phys. Rev. **162**, 549 (1967).

[26] E. R. Cowley, Solid Stat. Commu. **14**, 587.

[27] D. J. Scalapino, J. R. Schrieffer and J. W. Wilkins, Phys. Rev. **148**, 263 (1966).

[28] Y. Nakagawa and A. D. Woods, Phys. Rev. Lett. **11**, 271 (1963).

[29] J. Bostock, V. Diadiuk, W. N. Cheung, K. H. Lo, R. M. Rose and M. L. A. MacVicar, Phys. Rev. Lett. **36**, 603 (1976).

[30] G. B. Arnold, J. Zasadzinski and E. L. Wolf, Phys. Lett. **69A**, 136 (1978).

[31] K. E. Kihlstrom, D. A. Collins and S. I. Park, Phys. Rev. B **39**, 12257 (1989).

[32] W. H. Butler, F. J. Pinski and P. B. Allen, Phys. Rev. B **19**, 3708 (1979).

[33] L. Y. Shen, Phys. Rev. Lett. **24**, 1104 (1970).

[34] E. L. Wolf, R. J. Noer, D. Burnell and G. B. Arnold, J. Phys. F: Metal Phys. **11**, L23 (1981).

[35] J. Tuoriniemi, K. Juntunen-Nurmilaukas, J. Uusvuori, E. Pentti, A. Salmela and A. Sebedash, Nature **447**, 187 (2007).

[36] K. Shimitzu, H. Ishikawa, D. Takao, T. Yagi and K. Amaya, Nature **419**, 597 (2002).

[37] D. Kasinathan, K. Koepernik, J. Kuneš, H. Rosner and W. E. Pickett, Physica C **460-462**, 133 (2007).

[38] K. Shimitzu, T. Kimura, S. Furomoto, K. Takeda, K. Kontai, Y. Onuki and K. Amaya, Nature **412**, 316 (2001).

[39] S. Klotz and M. Braden, Phys. Rev. Lett. **85**, 3209 (2000).

[40] P. G. Tomlinson and J. P. Carbotte, Can. J. Phys. **55**, 751 (1977).

[41] M. Appapillai and A. R. Williams, J. Phys. F: Metal Phys. **3**, 759 (1973).

[42] F. J. Pinski, P. B. Allen and W. H. Butler, Phys. Rev. B **23**, 5080 (1981).

[43] H. K. Leung, J. P. Carbotte, D. W. Taylor and C. R. Leavens, Can. J. Phys. **54**, 1585 (1976).